Supramolecular Chemistry
Publication details, including instructions for authors and subscription information:
http://www.tandfonline.com/loi/gsch20

Synthesis of a novel pyrylium salt with chemoselectivity to a cyanide anion

Boddu Ananda Rao[a], Jae-Young Lee[a] & Young-A Son[a]
[a] Department of Advanced Organic Materials Engineering, Chungnam National University, 220 Gung-dong, Yuseong-gu, Daejeon305-764, South Korea
Published online: 25 Sep 2014.

Supramolecular Chemistry, 2015
Vol. 27, No. 3, 191–200, http://dx.doi.org/10.1080/10610278.2014.952297

Taylor & Francis
Taylor & Francis Group

Synthesis of a novel pyrylium salt with chemoselectivity to a cyanide anion

Boddu Ananda Rao, Jae-Young Lee and Young-A Son*

Department of Advanced Organic Materials Engineering, Chungnam National University, 220 Gung-dong, Yuseong-gu, Daejeon 305-764, South Korea

(*Received 5 February 2014; accepted 4 August 2014*)

The high-yield one-pot synthesis of a novel chemosensor based on a 4-methyl 2,6-diphenyl pyrylium trifluoromethanesulfonate (Pyr) salt that absorbs in the visible region is reported. The ability of pyr to sense various anions has been investigated using UV–visible spectroscopy and fluorescence spectroscopy. Pyr selectively detects CN^- in competition with various other anions such as Cl^-, Br^-, I^-, SCN^-, ClO_4^-, NO_3^-, HSO_4^- and PF_6^-, due to its highly reactive nature towards nucleophiles. The selective detection of CN^- with pyr gave rise to a significant hypochromic effect in CH_3CN solution at λ_{max} 387 and 446 nm, which are the absorption and fluorescence peaks, respectively. These studies indicated a high affinity of CN^- for pyr, and forming a 1:1 ratio leads to cyano-enone derivative.

Keywords: pyrylium trifluoromethanesulfonate; cyanide ion sensing; chemosensor; nucleophilic additions; pyrylium fluorescene

1. Introduction

The first **pyr** salt was isolated nearly 100 years ago. During the first half of this century, interest in these compounds was constant (*1*). **Pyr** salts represent a nodal point for many synthetic routes, more than any other heterocyclic systems. They can function as intermediates in an extraordinary variety of synthetic applications (*2–4*). These molecules are of considerable interest in theoretical, pharmaceutical and material chemistry, finding applications in many different areas. As versatile synthetic intermediates, these molecules are of practical interest for complex heterocyclic skeletons and for their intriguing physical properties. The electron-accepting nature of **pyr** salts has also resulted in diverse applications, such as their use as sensitisers for photoinduced electron transfer (PET) and as photocatalysts (*5,6*). **Pyr** salts are also used as fluorescence dye stuffs (*7,8*), non-linear optical (NLO) materials (*9,10*), phototherapeutics (*11–13*) and anticancer agents (*14*). The potential absorption, fluorescence and electron acceptor behaviour of **pyr** salts have been explored to design sensors for anions, amines (*15*), amino acids and proteins (*16*).

Pyr salts are playing an interesting role because they represent the extreme case of a single perturbation introduced by an heteroatom into a benzene ring, the replacement of CH in benzene O^+ modifies the electron distribution much more than any other common heteroatom (the electro negativity increases in the order $CR < N < NR^+ < O^+$), or than any substituent R in CR or NR^+. **Pyr** salts with heteroatoms being isoelectronic to the $-CH=$ group are subjects of greatest interest (*17*) due to their similarity to benzene from the point of view of raditional aromaticity criteria – presence of $(4n + 2)$ π-electrons within the cyclic conjugated system (*18*). They were expected to demonstrate similar physico-chemical properties and reactivity, taking into account perturbation of aromaticity caused by the presence of a heteroatom (*19*). Thus, **Pyr** salts give no electrophilic substitution, but the only addition of nucleophiles. Therefore, the structure and aromaticity of heterocyclic analogous of benzene have been widely investigated both experimentally and theoretically (see, for example, Refs. (*20, 21*) and references therein). Earlier reported methods for the preparation of **pyr** salts with different counter anions are not satisfactory, due to long synthetic sequences or low yields in the case of one-step processes, as shown in Chart 1. Various reported **pyr** salts include 4-methyl 2,6-diphenyl pyrylium tetrafluoroborate (*22–24*), 4-methyl 2,6-diphenyl pyrylium perchlorate (*23,25*), 4-methyl-2,6-diphenyl pyrylium aluminum tetrachloride (*26,27*), 4-methyl 2,6-diphenyl pyrylium iodide (*28,29*), 4-methyl 2,6-diphenyl pyrylium tetrachloroferrate (*30*), 4-methyl 2,6-diphenyl pyrylium chloroplatinate (*31*), 4-methyl 2,6-diphenyl pyrylium thiocyanate (*32*), 4-methyl 2,6-diphenyl pyrylium selenocyanate (*32*), 4-methyl 2,6-diphenyl pyrylium hexafluorophosphate (*33*) and 4-methyl 2,6-diphenyl pyrylium propanedinitrile, [(dicyanomethylene) amino] (*4*).

Cyanide is well known as one of the most toxic and extremely harmful materials to the environment and human health (*34*). The cyanide ion inhibits mitochondrial

*Corresponding author. Email: yason@cnu.ac.kr

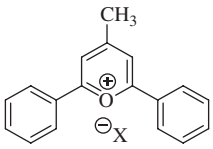

1 X = BF_4 **2** X = ClO_4
3 X = $AlCl_4$ **4** X = I
5 X = $FeClO_4$ **6** X = $PtCl_5$
7 X = SCN **8** X = SeCN
9 X = PF_6 **10** X = Propanedinitrile, [(dicyanomethylene)amino]

Chart 1. Pyrylium salts.

cytochrome oxidase and blocks electron transport, decreasing oxidative metabolism and oxygen utilisation (*35*); its accurate measurement is crucial in environmental control. Tobacco smoke is a common source of cyanide that can lead to high levels of this ion in the blood (*36*). Other potential sources of cyanide in humans and animals are sodium nitroprusside, succinonitrile and organic thiocyanates (*37*). The cyanide ion can affect many functions in the body, including the vascular, visual, central nervous, cardiac, endocrine and metabolic systems; exposure leads to vomiting, convulsions, the loss of consciousness and, eventually, death (*38–40*). The high level of intracellular calcium ion concentration is caused by the uptake of cyanide anions and triggers a cascade of enzymatic reactions to increase the level of reactive oxygen species, which finally inhibits the antioxidant defense system (*41*). Many analytical techniques, such as potentiometry, chromatography and flow injection, have been developed for cyanide detection (*42,43*). In addition, there have been a number of fluorescent chemosensors and chemodosimeters with selective sensing functions of the cyanide ion (*44,45*). Therefore, the selective and sensitive detection of cyanide is very important for environmental protection, food analysis and even anti-terrorism (*46,47*).

Recently, the use of **pyr** salt was reported for sensing the CN^- ion by nucleophilic addition (*48*). A particular feature of the cyanide ion, its nucleophilic character, enables this recognition system with some characteristic features. The formation of the C—C bond was observed in **pyr** salt-containing polymers as colourimetric sensors for cyanide ions. The electrophilic character of the **pyr** ring and the nucleophilicity of the cyanide ion combine to induce a remarkable colour change from yellow to red as a consequence of the formation of the cyano-enone derivative in CH_3CN solution (*49*). The applicability of thermally induced ring contractions for the convenient synthesis of (3,5-diaryl-2-furyl)(aryl) acetonitriles via the reaction of various 2,4,6-triaryl pyrylium perchlorates with sodium cyanide has been reported (*50*). Triaryl pyrylium perchlorates are readily converted into a new aromatic cyano-enones by using cyanide ion, as shown in Scheme 1 (*51*). Among other species tested, it was found that cyanide produced ring-open products. In a similar manner, the presence of primary aliphatic amines transformed the pyrylium ring into a pyridinium one (*52–55*). Pyrylium derivatives can be easily transformed into the parent thiopyrilium derivatives in the presence of sulfide anion (*4,56–58*).

In our earlier study, we have reported the synthesis of near-infrared absorbing pyrylium-squaraine dye for selective detection of mercury metal ion (*59*), colourimetric and 'turn-on' fluorescent determination of Hg^{2+} ions based on a rhodamine–pyridine derivative (*60*). Very recently, we have reported the synthesis and chemosensitivity of a new iminium salt towards a cyanide anion (*61*). On the basis of these previous reports, we are continuously exploring the synthesis and properties of new derivatives of **pyr** salts, which can potentially yield a new class of chromogens for the selective and quantitative detection of ions, both for biological and environmental applications. We have combined the capabilities of **pyr** salt and a suitable chromogenic organic group to develop new chromogenic compounds with enhanced sensing properties. Herein, we report the synthesis and binding properties of **pyr** chemosensors, along with their selective absorption and emission changes in the presence of cyanide. In this context, we have explored a new one-pot synthesis method for the preparation of the 4-methyl-2,6-di-phenyl-butyl pyrylium trifluoromethanesulfonate (**pyr**) salt using benzoyl chloride, anhydrous *t*-butyl alcohol and trifluoromethanesulfonic acid with high yields (>90%), as shown in Scheme 2.

2. Experimental section

2.1 *Chemical and starting materials*

All solvents and reagents (analytical grade and spectroscopic grade) were commercially purchased and used as received unless otherwise mentioned. The anions used in the form of tetra-butyl ammonium (TBA) salts, CF_3COOD, benzoyl chloride, trifluoromethanesulfonic acid and *t*-butyl alcohol were purchased from Sigma-Aldrich

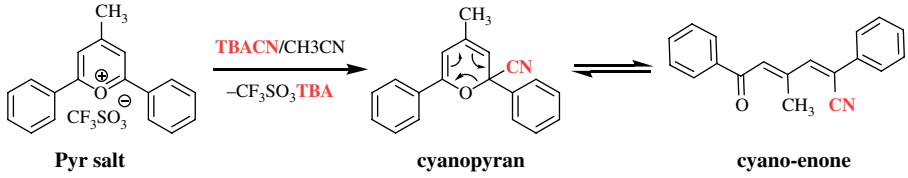

Scheme 1. (Colour online) A plausible mechanism for the formation of cyano-pyran and cyano-enone derivatives.

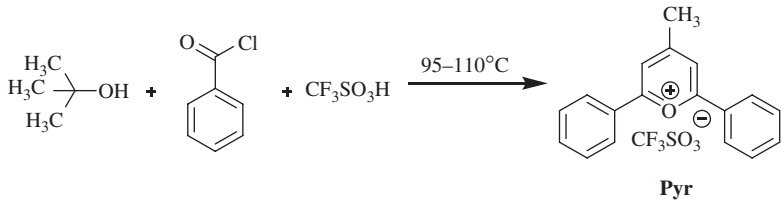

Pyr

Scheme 2. Synthesis of 4-methyl 2,6-diphenyl pyrylium trifluoromethanesulfonate (**Pyr**) salt.

and Alfa-Aesar Chemical Reagent Co. Water was purified and deionised (MilliQ grade, Millipore).

AVANCE III 600 Magnet: Ascend^{TM} series, 14.1 Tesla, ^{1}H resonance frequency 600 MHz, ^{13}C resonance frequency 150 MHz, Top Spin 3.1 (software) spectrometer (Germany) in CF_3COOD solvent. The chemical shifts (δ values) were reported in ppm down field from an internal standard (Me_4Si) (^{1}H and ^{13}C NMR). Mass spectra were recorded on a JEOL MStation [JMS-700] mass spectrometer. FTIR spectra were recorded with an FTS-175C spectrometer (Bio-laboratories, Cambridge, MA, USA). Melting points were recorded on a Bamstead electrothermal (UK) apparatus and are uncorrected. Elemental analyses were performed on a Carlo Elba Model 1106 analyser. UV–visible (UV–vis) absorption spectra were recorded on an Agilent 8453 spectrophotometer. Fluorescence emission spectra were recorded on a Shimadzu RF-5301PC spectroflurophotometer. HOMO/LUMO (highest occupied molecular orbital/lowest unoccupied molecular orbital) calculation and modelling simulations were conducted with DMol^3 of the *Material Studio 4.3 suite*.

2.2 General spectroscopic methods

TBA salts and **pyr** were dissolved in CH_3CN to obtain 1 mM (millimolar) stock solutions. Prior to spectroscopic measurements, the solution was freshly prepared by diluting the concentrated stock solution to the required concentration. All the experiments were conducted at standard barometric pressure and room temperature.

2.3 Synthesis of 4-methyl 2,6-di-phenyl-pyrylium trifluoromethanesulfonate (Pyr)

In a 500-mL three-neck round bottom flask equipped with a temperature probe, a magnetic stir bar and a nitrogen inlet adaptor with a dry ice condenser, 24 g (0.2 mol) of benzoyl chloride and 3.7 g (0.05 mol) of anhydrous *t*-butyl alcohol were loaded into the round-bottomed flask, and the condenser was filled with acetone and dry ice. The reaction mixture was heated to 95°C with stirring. Then, 15 g (0.1 mol) of trifluoromethanesulfonic acid was added with stirring over 2–3 min. After the addition was completed, the temperature was increased to 105–115°C and incubated for 20 min. The reaction mixture colour changed to brown, and the reaction was allowed to spontaneously cool to 50°C and finally cooled to −10°C with an ice and salt bath. While adding 100 mL of cold diethyl ether to the reaction mixture, a precipitate formed. After the precipitate formation, filtration was performed with a Buchner funnel, and the obtained solid was washed with diethyl ether (3 × 100 mL) and dried over P_2O_5 to give 17.86 g of the title compound (Yield 90.32%). The structure of **pyr** was confirmed by ^{1}H NMR, ^{13}C NMR, ESI-MS and FT-IR spectra (Figure S1–S4, Supplementary data).

Mp = 283–285°C; IR (KBr): 3072, 1629, 1518, 1271, 1148, 1030, 635 cm^{-1}; ^{1}H NMR (600 MHz, CF_3COOD): δ 3.26 (s, 3H), 8.08 (t, 4H, J = 7.34 Hz), 8.19 (t, 2H, J = 7.34 Hz), 8.59 (d, 4H, J = 3.76 Hz), 8.61 (s, 2H) ppm; ^{13}C NMR (150 MHz, CF_3COOD): δ 25.1, 121.1, 130.1, 130.4, 132.7, 138.6, 174.2, 176.4 ppm. ESI-MS (*m/z*): 247.3 $[M]^+$(100) for pyrylium cation and 148.9 $[M]^+$(100) for trifluoromethanesulfonate anion. Elemental analysis calculated (%) for $C_{19}H_{15}F_3O_4S$: C, 57.57; H, 3.81; F, 14.38; O, 16.15; S, 8.09; found: C, 57.43; H, 3.85; F, 14.31; O, 16.43; S, 7.98.

3. Results and discussion

3.1 Spectroscopic measurements

To develop an efficient anion receptor for the cyanide (CN^-) ion, **pyr** was prepared and its interaction with various anions was analysed in solution via spectrophotometric titrations. **Pyr** exhibited poor solubility in water (H_2O) solvent and good solubility in acetonitrile (CH_3CN) solvent. First, we tested the CN^- ion (40 μM) with **pyr** (40 μM) in H_2O solvent to select a solvent system. In this experimental study, the selectivity test was carried out using **pyr** (40 μM) salt as probe in the water solvent system with different anions (40 μM) like CN^-, Cl^-, Br^-, I^-, SCN^-, ClO_4^-, NO_3^-, HSO_4^- and PF_6^-. While 1 equiv of CN^- (40 μM) with respect to **pyr** (40 μM) was added to the solution, colour changes were not identified by the naked eye. In the case of fluorescence under a 365-nm UV lamp, the **pyr** was selective towards other anions also as shown in Figure S5, Supplementary data. The addition of the anions (1 equiv) did not produce any apparent colour or spectral change. **Pyr** (40 μM, H_2O) exhibits an absorption band at λ_{max} 387 nm in UV–vis spectroscopy.

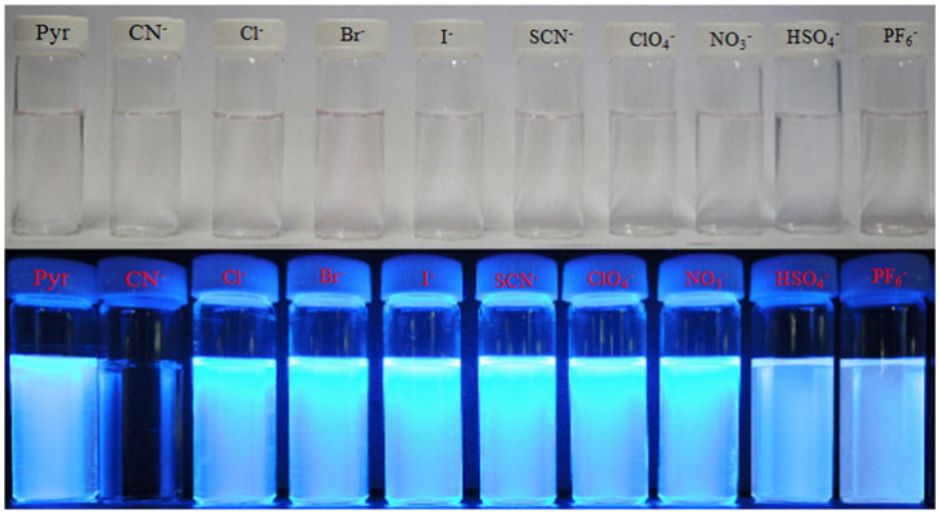

Figure 1. (Colour online) Photo images with no magnification (top picture) and fluorescence under 365-nm UV lamp colour changes (bottom picture) by adding various anions (40 μM) to the solutions of **pyr** (40 μM) in CH_3CN solutions. **Pyr**, CN^-, Cl^-, Br^-, I^-, SCN^-, ClO_4^-, NO_3^-, HSO_4^- and PF_6^- (from left to right).

With the addition of TBA salts with anions CN^-, Cl^-, Br^-, I^-, SCN^-, ClO_4^-, NO_3^-, HSO_4^- and PF_6^- (1 equiv) to the solution, this absorption band has not completely disappeared, even in the case CN^- ion also as shown in Figure S6, Supplementary data. The sensing activity was predominantly observed by adding various anions in the form of TBA salts (CN^-, Cl^-, Br^-, I^-, SCN^-, ClO_4^-, NO_3^-, HSO_4^- and PF_6^-) to **pyr** salt in CH_3CN solution. When 1 equiv of CN^- (40 μM) with respect to **pyr** salt (40 μM) was added to the solution, colour changes were not identified by the naked eye. Interestingly, in the case of fluorescence under a 365-nm UV lamp, the **pyr** salt changed colour from bright blue fluorescence to colourless as shown in Figure 1. Next, we compared the sensing behaviour of **pyr** towards CN^- ion with two different solvent systems such as H_2O and CH_3CN. **Pyr** in CH_3CN solvent was selectively sensing the CN^- anion. But in the case of H_2O solvent, the **pyr** was not effective towards colour variations as shown in Figure S7, Supplementary data. **Pyr** (40 μM, CH_3CN & H_2O) exhibits an absorption band at λ_{max} 387 nm in the UV–vis spectra. After adding CN^- (40 μM) anion to the **pyr** (40 μM) in CH_3CN solvent, the absorption band completely disappeared, and additionally a new peak was observed at λ_{max} 316 nm. But in the case of H_2O as a solvent, λ_{max} 387 nm absorption band was not completely quenched and does not generate new peak as shown in Figure S8, Supplementary data. These results strongly support that the CH_3CN is the best solvent over water. Later, we recorded UV–vis spectral studies for cyanide anion sensing behaviour towards **pyr** in mixed organic aqueous solutions such as H_2O and CH_3CN solvents as shown in Figure S9, Supplementary data. In this experiment, **pyr** (40 μM) towards CN^- ion (40 μM) with varying H_2O:CH_3CN ratios (10:0 to 0:10; v/v) via absorption spectroscopy was tested. Even H_2O:CH_3CN (10:0 to 1:9; v/v) CN^- ion has not completely quenched the absorption band at λ_{max} 387 nm. When H_2O:CH_3CN is in the ratio of 0:10 (v/v) ratio, absorption band λ_{max} 387 nm was completely quenched and generated new peak at λ_{max} 316 nm. These results are shown CH_3CN solvent is better than mixed organic aqueous solutions. Other experiments further demonstrated the selectivity of the complex formation of **pyr** salt with the cyanide ion. Herein, we report the interesting experimental results in detail.

Pyr salt (40 μM, CH_3CN) exhibits an absorption band at λ_{max} 387 nm. Upon addition of TBA salts with anions CN^-, Cl^-, Br^-, I^-, SCN^-, ClO_4^-, NO_3^-, HSO_4^- and PF_6^- (1 equiv.) to the solution, this absorption band completely disappeared only with the CN^- ion, and in addition a new peak was observed at 316 nm. (see Figure 2(A)). The addition of the other anions (1 equiv) did not produce any apparent colour or spectral change. Similarly, in the case of fluorescence spectra, a pure **pyr** (40 μM, CH_3CN) solution displays an emission peak at 446 nm upon excitation at λ_{max} 387 nm. During the addition of various anions to the **pyr** solution, emission peaks were observed at 446 nm, except with the addition of the cyanide anion. Experimental results show that the complete quenching of the emission peak at 446 nm was only observed with cyanide ion (Figure 2(B)). One of the most characteristic properties of the **pyr** ring that was observed is nucleophilic addition, and this selectivity of **pyr** towards CN^- in CH_3CN solution can be reasonably assumed to be due to the stronger nucleophilicity of the cyanide ion.

The gradual addition of CN^- (0–1.5 equiv) to a solution of **pyr** (40 μM, CH_3CN) caused the gradual decrease in absorbance intensity at 387 nm. In addition, a new peak at 316 nm is shown in Figure 3(A) absorption

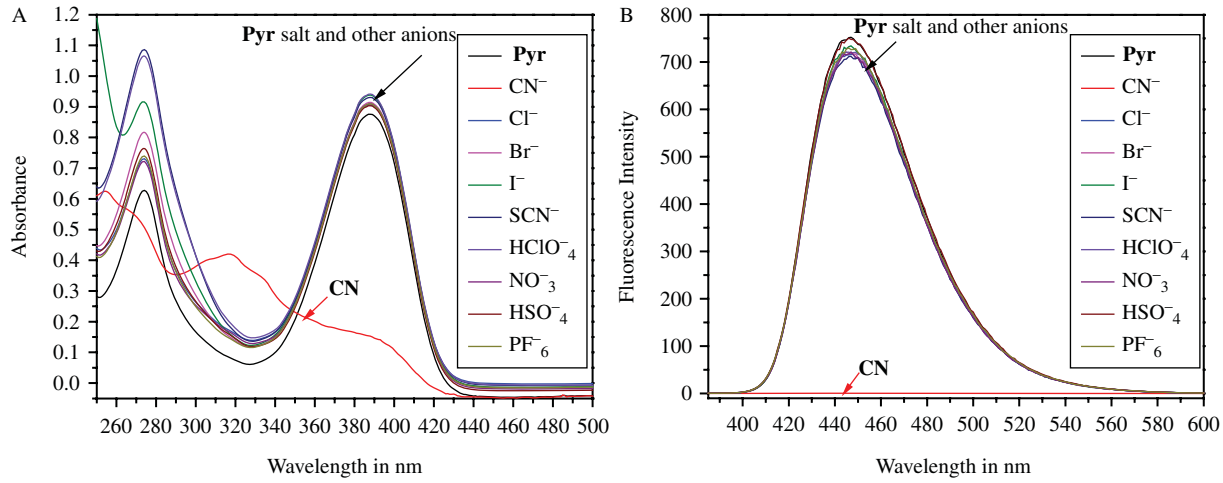

Figure 2. (Colour online) (A) Absorption and (B) fluorescence spectra of the **pyr** salt (40 μM) with different anions (40 μM) in CH_3CN solutions.

spectra along with isosbestic point through 347 nm. When the concentration of the CN^- reached 1 equiv with respective to the **pyr**, the absorption peak at 387 nm entirely disappeared and was invariably preserved upto 1.5 equiv The **pyr** salt exhibited good fluorescence properties and quantum yield. Accordingly, as shown in Figure 3(B) fluorescence spectra, upon excitation at 380 nm, the free **pyr** (40 μM, CH_3CN) displays a single emission band centred at 446 nm. The gradual addition of CN^- (0–1.5 equiv) decreased the fluorescence intensity at approximately 446 nm. Primarily with the addition of 0.4 equiv of cyanide ion, the fluorescence intensity slightly increased and then regularly decreased with increasing amounts of CN^-. With 1.2 equiv of CN^-, the ion emission peak intensity was fixed, and no changes were observed in the fluorescence intensity of the **pyr** salt. The titration of **pyr** with CN^- in CH_3CN shows the formation of 1:1 complexes, as indicated by the absorption and fluorescence spectra insets. The absorption and fluorescence spectra of the **pyr** salt are due to the presence of a positive charge on oxygen and a lone pair of electrons not participating in excitations. No lower energy $n \rightarrow \pi^*$ transitions were observed; therefore, it was inferred that the lower energy transitions were of type $\pi \rightarrow \pi^*$. On the basis of the results obtained above, a potential binding mechanism involves the formation of cyano pyran in the first step, which is readily converted into a cyano-enone derivative through a tautomeric process (see Scheme 1) (*50*).

Quantum yields were measured in CH_3CN relative to 9,10-diphenylanthracene (DPA) (0.9 in cyclohexane,

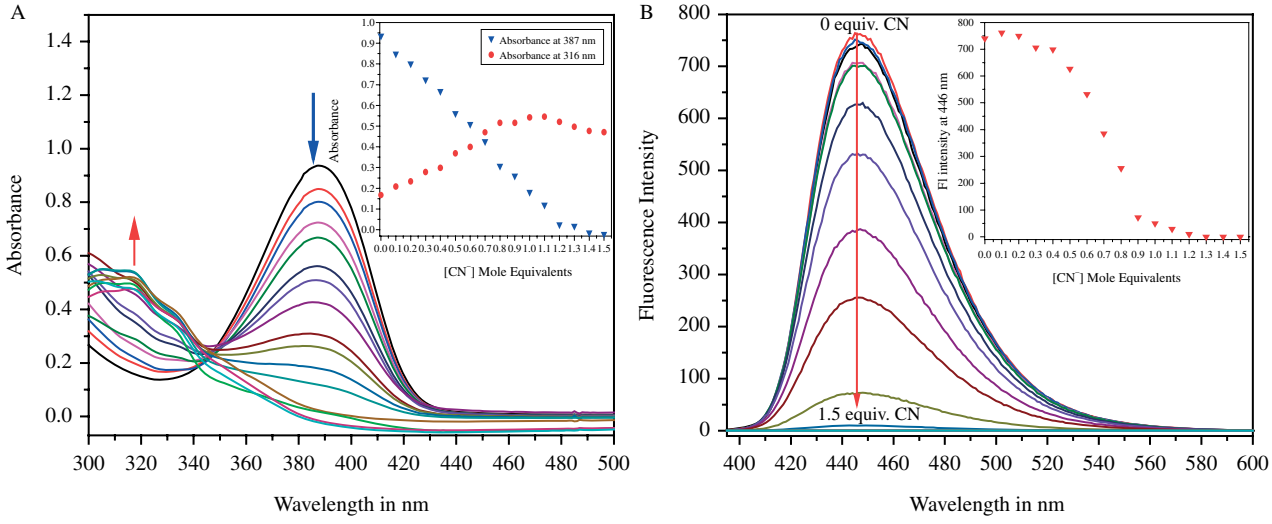

Figure 3. (Colour online) (A) Absorption and [B] fluorescence spectra of the **pyr** salt (40 μM) with various concentrations of CN^- (0–1.5 equiv) in CH_3CN solutions.

Table 1. Calculated molar extension coefficients (ε_{max}) and quantum yields (Φ) for the **pyr** salt towards different concentrations of the CN^- ion.

Entry	Concentration of CN^- (10 μM)	Absorbance of Pyr (40 μM)	ε_{max} ($M^{-1}cm^{-1}$) (10^5)	Quantum yield (Φ_F) in %
1	0.4	0.8488	2.122	76.81
2	0.8	0.8016	1.002	75.45
3	1.2	0.7246	0.6038	74.36
4	1.6	0.6678	0.4173	69.57
5	2	0.5613	0.2806	68.42
6	2.4	0.5095	0.2122	66.42
7	2.8	0.4262	0.1522	40.58
8	3.2	0.3075	0.0960	25.71
9	3.6	0.2603	0.0723	8.32
10	4	0.1813	0.0453	3.83

Absorption of **pyr** salt $\lambda_{max} = 387$ nm; fluorescence excitation $\lambda_{max} = 380$ nm; fluorescence emission $\lambda_{max} = 446$ nm.

fluorescence emission range λ_{max} 400–500 nm and useful excitation range 320–370 nm), as shown in Table 1 (*62*). The quantum yield of the standard samples, which have a fixed and known fluorescence quantum yield (Φ) value, was calculated according to the following Equation (1):

$$\Phi = \Phi S \frac{I}{I_S}\frac{A_S}{A}\frac{\eta^2}{\eta_S^2}, \quad (1)$$

where Φ is the quantum yield of the **pyr** salt towards different concentrations of CN^- ion; Φ_S is standard DPA (0.9 in cyclohexane); I is the integral area of the compound in emission spectra; I_S is the integral area of the standard DPA in emission spectra; A_S is the absorbance of the standard DPA; A is the absorbance of the compound; η is the refractive index of the solvent used for the compound (CH_3CN) and η_S is the refractive index of the solvent used for the standard DPA (cyclohexane).

Different concentrations of CN^- ion influenced the molar extension coefficients (ε_{max}) and the quantum yields (Φ) of the **pyr** salt, as shown in Table 1. The maximum molar extension coefficient and quantum yield occurred with 0.4 equiv of CN^- ion and decreased as the concentration of the CN^- ion increased from 0.4 to 1 equiv This indicates the formation of a 1:1 complex between CN^- ion and **pyr** salt because the minimum absorption coefficient and quantum yield were obtained with 1 equiv of CN^- (40 μM) and 1 equiv of **pyr** salt (40 μM).

The binding stoichiometry between **pyr** salt and the CN^- ion is essential to understand its sensing properties. With regard to this point, Job's plot method showed a 0.5 stoichiometric ratio for **pyr** salt and CN^- ion complex formation, as shown in the A_0/A at 387 nm (Figure 4(A)) and the fluorescence intensity I_0/I at 446 nm in CH_3CN (Figure 4(B)). The absorption and fluorescence intensities were plotted against different molar fractions of **pyr** salt and CN^- ion, showing their maximum intensity was reached with a 0.5 stoichiometry ratio from Job's plot analysis. These results also indicate a 1:1 ratio. This result shows that the positive charge on the oxygen atom of **pyr** salt attracts the nucleophilic CN^- ion (1 equiv) and leads to the formation of a cyano–pyran resonance structure.

The high selectivity of **pyr** salt for CN^- was demonstrated further in extreme competition. Among nine different anions screened under identical conditions, including Cl^-, Br^-, I^-, SCN^-, ClO_4^-, NO_3^-, HSO_4^- and PF_6^-, the absorption response of **pyr** was exclusively observed with CN^-, with a consistent hypochromic effect at 387 nm (Figure 5(A)). A solution of **pyr** was treated with all nine different anions in combination, which showed only a weak background signal in absorption intensity at 387 nm. As shown in Figure 5(B), a consistent quenching of the fluorescence intensity at 446 nm was also observed in competition studies when CN^- was

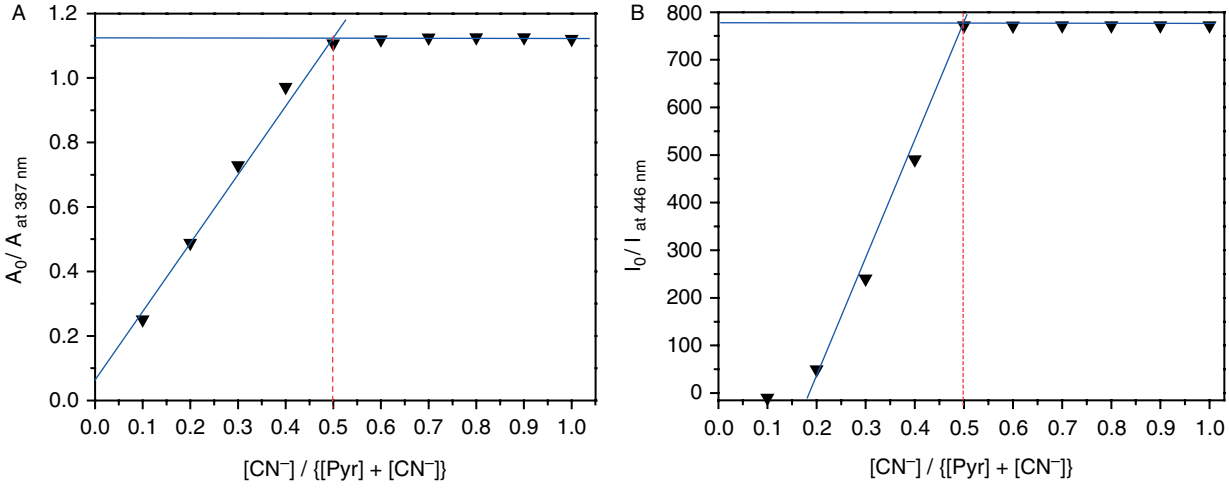

Figure 4. (Colour online) (A) Absorption and (B) fluorescence spectra in Job's plot method of the **pyr** salt with CN^- in CH_3CN solution.

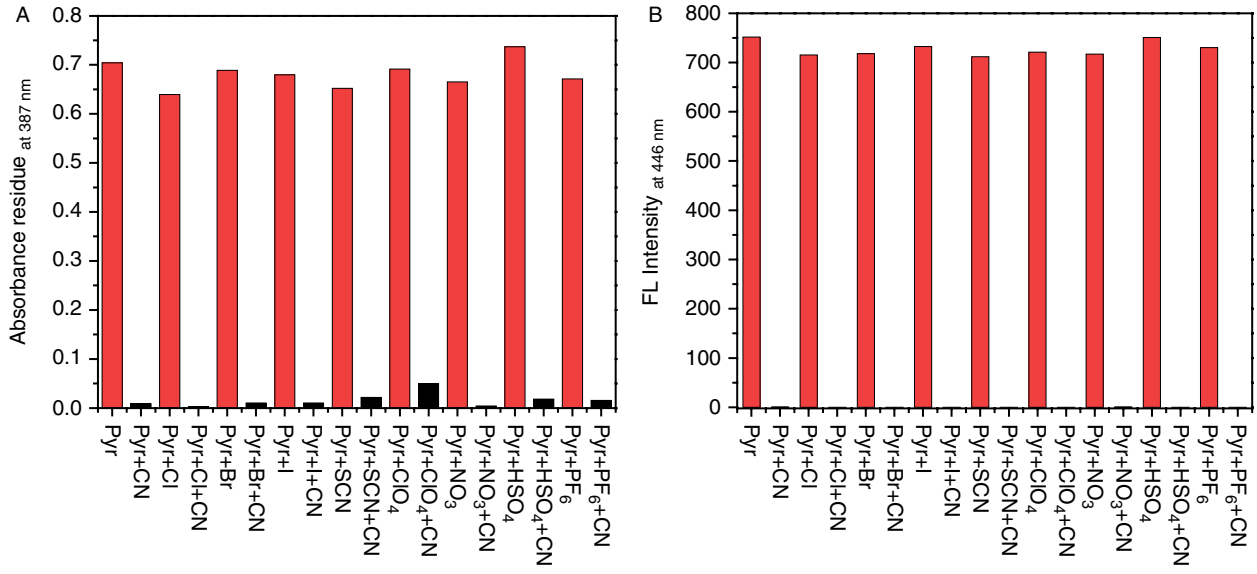

Figure 5. (Colour online) Sensitisation competition between the CN^- ion with different anions, such as Cl^-, Br^-, I^-, SCN^-, ClO_4^-, NO_3^-, HSO_4^- and PF_6^-. The red bars represent the absorption and emission of **pyr** in the presence of 1 equiv of the anion of interest. The black bars indicate the change in the (A) absorption (387 nm) and (B) fluorescence (446 nm) that occurs upon the addition of 1 equiv of CN^- to the solution containing **pyr** and the anion of interest. Conditions: $\lambda_{exc} = 380$ nm; $T = 298$ K; CH_3CN.

subsequently added to the solutions containing other anions. Upon the addition of CN^- ion to this mixture, an immediate quenching in the fluorescence intensities was observed. The absorption and fluorescence detection of CN^- by **pyr** (Figure 5) relies critically on the clean and fast C − C bond formation under ambient conditions (see Scheme 1). This finding demonstrates the unique selectivity of **pyr** salt towards CN^- ion.

One particular feature of the CN^- ion reactivity with the **pyr** ring is that the process is reversible, and it has been reported that in the presence of acidic solution, the **pyr** derivative could be retrieved. Therefore, the attractive possibility of attaining reusable colourimetric **pyr** salt was tested via the recuperation of the sensing **pyr** by reaction of the cyano-enone derivative with acidic solutions. **Pyr** salt, saturated with CN^- was added to aqueous hydrochloric acid (40 μM), and the recovery of the original colour of the **pyr**-containing solution was observed for absorption (Figure 6(A)) and fluorescence (Figure 6(B)) spectra. This acid treatment also reverted the

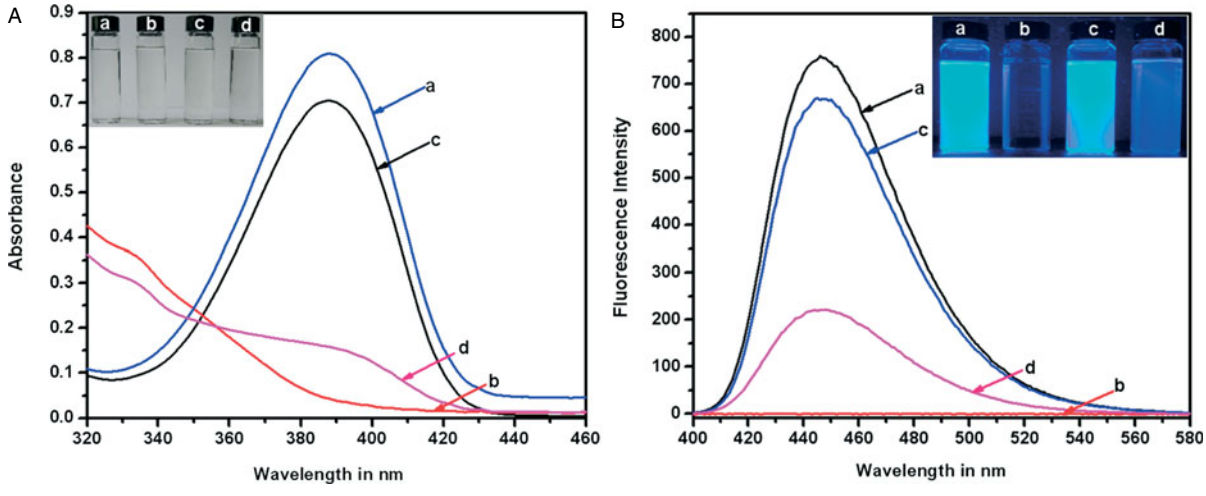

a) Pyr; b) Pyr + CN^-; c) Pyr + CN^- + HCl; d) Pyr + CN^- + HCl + CN^-

Figure 6. (Colour online) (A) Absorption at 380 nm and (B) fluorescence at 446 nm of the pure **pyr** salt (40 μM), which was lost with the addition of CN^- (40 μM), rescued with an acidic HCl aqueous solution (40 μM) and diminished again with another equivalent of CN^- (40 μM).

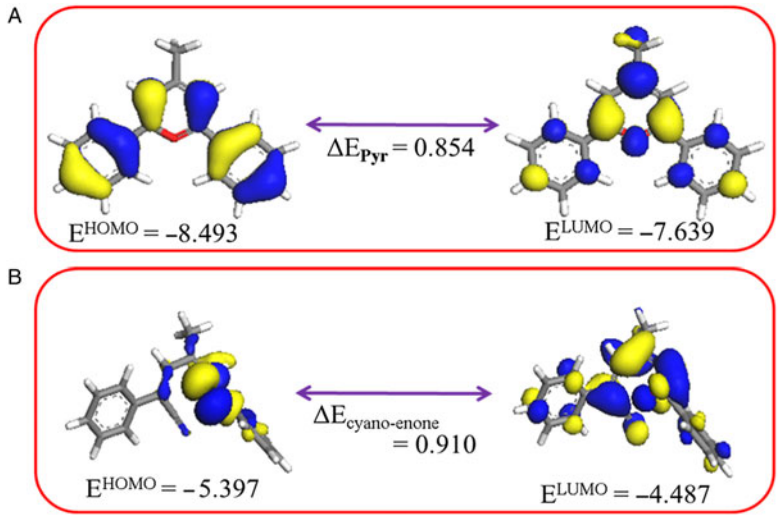

Figure 7. (Colour online) Electron distributions of the HOMO and LUMO energy levels; (A) pure **pyr** salt and (B) the cyano-enone derivative.

ring opening caused by the HCl. In the absorption spectra, the pure **pyr** salt absorbance at 387 nm underwent a hypochromic effect after adding CN^- ion. To this cyano-enone derivative (saturated) solution, the addition of hydrochloric acid solution rescued the original absorbance of the **pyr** salt. Finally, with the addition of a second equivalent of CN^- to the HCl solution, the absorbance of the **pyr** salt was not completely restored to that of the pure **pyr** salt. The trifluoromethanesulfonic acid (Triflic acid, super acid) (*63, 64*) that formed when the HCl solution was added might not be neutralised by the second equivalent CN^- ion. Thus, the hypochromic effect does not occur after the addition of a second equivalent of CN^- ion (shown in Scheme 1). The same results were obtained from the fluorescence spectra and are also shown in Figure 6(A) and (B) insets. These studies demonstrated the regeneration of **pyr** salt by hydrochloric acid from a cyano-enone (saturated) solution.

3.2 *Computational studies*

Finally, computational calculations have been carried out to investigate the binding mechanism and HOMO/LUMO energy levels of **pyr** salt and the cyano-enone derivative (Figure 7). These have been simulated with *Material Studio 4.3 suite*, which is a quantum mechanical method using the density functional theory. The Perdew–Burke–Ernzerhof function of the generalised gradient approximation level with a double numeric polarisation basis set has been used to calculate the energy level of the frontier molecular orbitals (MOs) (*65–69*). The comparison of the electron distribution of the HOMO and LUMO states in **pyr** and cyano-enone derivative showed that electron density decreased in LUMO levels compared to HOMO levels in the **pyr** ring structure, as shown in Figures 7(A) and (B). The energy gap between the HOMO and LUMO levels is 0.854 eV and 0.91 eV with **pyr** and the cyano-enone derivative, respectively. According to the experimental results, the hypsochromic (blue) shifts of the cyano-enone derivative can be attributed to the decrease in the HOMO–LUMO gap from **pyr** to the cyano-enone derivative. It is our experience that the most characteristic properties of the **pyr** rings are their ability to engage in nucleophilic addition reactions. Therefore, the clean and fast C − C bond forming reaction and the formation of a ring-opened product should be observed. This attack results in the opening of the **pyr** ring and produces a cyano-pyran moiety that is in equilibrium with the corresponding cyano-enone tautomer.

4. Conclusion

In conclusion, we have synthesised and demonstrated the novel use of a **pyr** salt as a dual-mode sensor for the detection of CN^- in CH_3CN solutions. The optical properties of this **pyr** salt were investigated with various anions, such as CN^-, Cl^-, Br^-, I^-, SCN^-, ClO_4^-, NO_3^-, HSO_4^- and PF_6^-. The results showed the enhanced sensitivity and the significant selectivity in the preference for CN^- over other anions. The stoichiometry of the complex between the **pyr** salt and CN^- was revealed to be 1:1, and cyano-enone derivative formation coincided with a colour change from bright blue fluorescence to colourless. Fluorescence studies revealed that a 387-nm absorption peak is responsible for the emission peak at 446 nm. UV–vis and fluorescence spectra revealed a hypochromic effect after the addition of CN^- ion to the **pyr** salt. In addition, a new peak at 316 nm is shown in

absorption spectra along with isosbestic point with 347 nm. In this pattern, selective binding leads to ~71 nm [387 − 316 nm] hypsochromic (blue) shift. The attractive possibility of attaining a reusable colourimetric **pyr** salt was tested via the reaction of the cyano-enone derivative with acidic solutions to obtain the former **pyr** salt. The reaction is reversible, and the sensor **pyr** salt can be recovered by adding aqueous hydrochloric acid. In this study, we summarised the computational studies of the **pyr** salt and the cyano-enone derivative to understand electronic distribution in the HOMO and LUMO levels. From our findings, theoretical approaches were compared to consider more detailed characteristics of the **pyr** salt and the cyano-enone derivative formation. Further studies are in progress to understand the effects of various substituent's on anion recognition and to develop **pyr**-based sensors for important anions.

Supplementary data

The ^{1}H NMR, ^{13}C NMR, FT-IR and mass spectra data for the **pyr** salt are available. Supplementary data associated with this article can be found here: http://dx.doi.org/10.1080/10610278.2014.952297.

Funding

This study was supported by the Basic Science Research Program through the National Research Foundation of Korea (NRF) funded by the Ministry of Education, Science and Technology [grant number 2013054767].

References

(1) Balaban, A.T.; Schroth, W.; Fischer, G. Journal of Luminescence Advances in Heterocyclic Chemistry. Academic Press: New York, NY, 1969; 10, pp 241–326.
(2) Balaban, A.T.; Dinculescu, A.; Dorofeenko, G.N.; Fischer, G.W.; Koblik, A.V.; Mezheritskii, V.V.; Schroth, W. Katritzky, A.R., Ed.; Academic Press: New York, NY, 1982; Vol. 2, p 454.
(3) Balaban, A.T., Chizov, O., Eds.; *Organic Synthesis: Modern Trends*, Proc. 6th IUPAC Internat. Symp. On Organic Synthesis, Moscow, 1987; pp 263–274.
(4) Balaban, T.S.; Balaban, A.T. *Science of synthesis: Houben-Weyl Methods of Molecular Transformations*; Georg Thieme Verlag: Stuttgart, 2003; 14, pp 11–200.
(5) Bogatian, M.V.; Simion, D.; Corbu, A.C.; Deleanu, C.; Chiraleu, F.; Maganu, M.; Bogatian, G. *Rev. Roum. Chim.* **2002**, *51* (4), 273–281.
(6) Bogatian, M.V.; Corbu, A.C.; Deleanu, C.; Chiraleu, F.; Maganu, M.; Bogatian, G. *Rev. Roum. Chim.* **2007**, *52* (1–2), 181–187.
(7) Polyzos, I.; Tsigaridas, G.; Fakis, M.; Giannetas, V.; Persephon, P. *J. Phys. Chem. B* **2006**, *110*, 2593–2597.
(8) Pigliucci, A.; Nikolov, P.; Rehaman, A.; Gagliardi, L.; Cramer, C.J.; Vauthey, E. *J. Phys. Chem. A* **2006**, *110*, 9988–9994.
(9) Andreu, R.; Galan, E.; Garın, J.; Herrero, V.; Lacarra, E.; Orduna, J.; Alicante, R.; Villacampa, B. *J. Org. Chem.* **2010**, *75*, 1684–1692.
(10) Andreu, R.; Carrasquer, L.; Franco, S.; Garın, J.; Orduna, J.; Martinez de Baroja, M.; Alicante, R.; Villacampa, B.; Allain, M. *J. Org. Chem.* **2009**, *74*, 6647–6657.
(11) Sawada, G.A.; Raub, T.J.; Higgins, J.W.; Brennan, N.K.; Moore, T.M.; Tombline, G.; Detty, M.R. *Bioorg. Med. Chem.* **2008**, *16*, 9745–9756.
(12) Holt, J.J.; Gannon, M.K.; Tombline, G.; McCarty, T.A.; Page, P.M.; Bright, F.V.; Detty, M.R. *Bioorg. Med. Chem.* **2006**, *14*, 8635–8643.
(13) Wagner, S.J.; Akripchenko, S.; Donnelly, D.J.; Ramaswamy, K.; Detty, M.R. *Bioorg. Med. Chem.* **2005**, *13*, 5927–5935.
(14) Tadashi, O.; Nobuko, Y.; Masahiro, K. *U.S. Patent* **2001**, *6*, 242–477.
(15) Ilies, M.A.; Seitz, W.A.; Ghiviriga, I.; Johnson, B.H.; Miller, A.; Thompson, E.B.; Balaban, A.T. *J. Med. Chem.* **2004**, *47*, 3744–3754.
(16) Wetzl, B.K.; Yarmoluk, S.M.; Craig, D.B.; Wolfbeis, O.S. *Angew. Chem. Int. Ed.* **2004**, *43*, 5400–5402.
(17) Balaban, A.T.; Krygowski, T.M.; Cyranski, M.K. *Topics in heterocyclic chemistry 19, aromaticity in heterocyclic compounds*; Springer: New York, NY, 2008; pp 203–246.
(18) Huckel, E.Z. *Z. Phys.* **1932**, *76*, 628–648.
(19) Balaban, A.T.; Oniciu, D.C.; Katritzky, A.R. *Chem. Rev.* **2004**, *104*, 2777–2812.
(20) Balaban, A.T.; Krygowski, T.M.; Cyranski, M.K. *Topics in heterocyclic chemistry 19, aromaticity in heterocyclic compounds*; Springer: New York, NY, 2008; pp 203–246.
(21) Krygowski, T.M.; Cyranski, M.K. *Topics in heterocyclic chemistry 19, aromaticity in heterocyclic compounds*; Springer: New York, NY, 2009; pp 1–344.
(22) Doddi, G.; Ercolani, G. *Synth. Commun.* **1987**, *17*, 817–818.
(23) Mori, A.; Kanemasa, S.; Wada, E.; Fujimoto, E.; Takeshita, H.; Kato, N.; Mori, A. *Heterocycles* **1993**, *35*, 869–878.
(24) Boiko, I.I.; Dergunova, M.E.; Boiko, T.N. *Chem. Heterocycl. Compd.* **1987**, *23*, 1169–1171.
(25) Katritzky, A.R.; Du, W.; Denisenko, S.N. *J. Prakt. Chem.* **1999**, *341*, 152–158.
(26) Hofelschweiger, B.K. Doctoral thesis, Universitätsbibliothek Regensburg, Regensburg, Germany, **2005**.
(27) Gray, A.P.; Archer, W.L. *J. Am. Chem. Soc.* **1957**, *79*, 3554–3559.
(28) Dimroth, V.K.; Arnoldy, G.; Eicken, S.V.; Schiffler, G. *Justus Liebigs Ann. Chem.* **1957**, *604*, 21–51.
(29) Balaban, A.T.; Mocanu, M.; Simon, Z. *Tetrahedron* **1964**, *20*, 119–130.
(30) Dimroth, V.K.; Wolf, K.; Kroke, H. *Justus Liebigs Ann. Chem.* **1964**, *678*, 183–201.
(31) Balaban, A.T.; Nenitzescu, C.D. Aluminiumchlorid-katalysen. *Justus Liebigs Ann. Chem.* **1959**, *625*, 74–88.
(32) Badilescu, S.; Balaban, A.T. *Spectrochim. Acta A Mol. Biomol. Spectrosc.* **1976**, *32A*, 1311–1318.
(33) Dave, K.; Scozzafava, A.; Vullo, D.; Supuran, C.T.; Ilies, M.A. *Org. Biomol. Chem.* **2011**, *9*, 2790–2800.
(34) Ma, J.; Dasgupta, P.K. *Anal. Chim. Acta* **2010**, *673*, 117–125.
(35) Camerino, P.W.; King, T.E. *J. Biol. Chem.* **1966**, *241*, 970–979.
(36) Xu, Z.; Chen, X.; Kim, H.N.; Yoon *J. Chem. Soc. Rev.* **2010**, *39*, 127–137.
(37) World Health Organization, guidelines for drinking-water quality. Geneva, Switzerland, **1996**.

(38) Kyung-Sik, L.; Hae-Jo, K.; Gun-Hee, K.; Injae, S.; Jong-In, H. *Org. Lett.* **2008**, *10*, 49–51.
(39) Park, S.; Kim, H.J. *Sens. Actuator B*. **2012**, *161*, 317–321.
(40) Park, S.; Kim, H.J. *Sens. Actuator B*. **2012**, *168*, 376–380.
(41) Lee, J.H.; Jeong, A.R.; Shin, I.S.; Kim, H.J.; Hong, J.I. *Org. Lett.* **2010**, *12*, 764–767.
(42) Pecharroman, B.V.; Lugue de Castro, M.D. *Analyst* **2002**, *127*, 267–270.
(43) Giuriati, C.; Cavalli, S.; Gorni, A.; Badocco, D.; Pastore, P. *J. Chromatogr. A*. **2004**, *1023*, 105–112.
(44) Isaad, J.; Achari, A.E. *Tetrahedron* **2011**, *67*, 5678–5685.
(45) Sumiya, S.; Doi, T.; Shiraishi, Y.; Hirai, T. *Tetrahedron* **2012**, *68*, 690–696.
(46) Na, S.Y.; Kim, J.Y.; Kim, H.J. *Sens. Actuator B.* **2013**, *188*, 1043–1047.
(47) Kim, G.J.; Kim, H.J. *Tetrahedron Lett.* **2010**, *51*, 185–187.
(48) Heidarizadeh, F.; Abadast, F. *Orient. J. Chem.* **2011**, *27*, 1421–1436.
(49) Garcia, F.; Garcia, J.M.; Garcia-Acosta, B.; Martinez-Manez, R.; Sancenon, F.; Soto, J. *Chem. Commun.* **2005**, *22*, 2790–2792.
(50) Mouradzadegun, A.; Abadast, F. *Tetrahedron Lett.* **2013**, *54*, 2641–2644.
(51) Mouradzadegun, A.; Abadast, F. *Monatsh. Chem.* **2013**, *144*, 375–379.
(52) Azab, H.A.; El-Korashy, S.A.; Anwar, Z.M.; Khairy, G.M.; Duerkop, A. *J. Photochem. Photobiol.* **2012**, *243*, 41–46.
(53) Garcıa-Acosta, B.; Comes, M.; Bricks, J.L.; Kudinova, M.A.; Kurdyukov, V.V.; Tolmachev, A.I.; Descalzo, A.B.; Marcos, M.D.; Martınez-Manez, R.; Moreno, A.; Sancenon, F.; Soto, J.; Villaescusa, L.A.; Rurack, K.; Barat, J.M.; Escriche, I.; Amoros, P. *Chem. Commun.* **2006**, 2239–2241.
(54) Comes, M.; Marcos, M.D.; Martinez-Manez, R.; Millan, M.C.; Ros-Lis, J.V.; Sancenon, F.; Soto, J.; Villaescusa, L.A. *Chem. Eur. J.* **2006**, *12*, 2162–2170.
(55) Moghimia, A.; Maddahb, B.; Yarib, A.; Shamsipurb, M.; Boostania, M.; Fall Rastegarc, M.; Ghaderi, A.R. *J. Mol. Struc.* **2005**, *752*, 68–77.
(56) Bicker, K.; Wiskur, S.L.; Lavigne, J.J. Colorimetric sensor design, in chemosensors: principles, strategies, and applications. In *Wiley series in drug discovery and development*; Wang, B., Anslyn, E.V., Eds.; Wiley: New York, 2011.
(57) Jimenez, D.; Martınez-Manez, R.; Sancenon, F.; Ros-Lis, J.V.; Benito, A.; Soto, J. *J. Am. Chem. Soc.* **2003**, *125*, 9000–9001.
(58) Garcıa-Acosta, B.; Garcıa, F.; Garcıa, J.M.; Martınez-Manez, R.; Sancenon, F.; San-Jose, N.; Soto, J. *Org. Lett.* **2007**, *9*, 2429–2432.
(59) Boddu, A.R.; Kim, H.; Son, Y.A. *Sens. Actuator, B.* **2013**, *188*, 847–856.
(60) Lee, S.H.; Boddu, A.R.; Son, Y.A. *Sens. Actuators, A.* **2014**, *196*, 388–397.
(61) Boddu, A.R.; Lee, J.Y.; Son, Y.A. *Spectrochim. Acta, Part B*. **2014**, *127*, 268–274.
(62) Hamal, S.; Hirayama, F. *J. Phys. Chem.* **1983**, *87*, 83–89.
(63) Fabes, L.; Swaddle, T.W. *Can. J. Chem.* **1975**, *53*, 3053–3059.
(64) Gramstad, T.; Haszeld, R.N. *J. Chem. Soc.* **1957**, 4069–4079.
(65) Yan, D.; Lu, J.; Ma, J.; Wei, M.; Li, S.; Evans, D.G.; Duan, X. *J. Phys. Chem. C*. **2011**, *115*, 7939–7946.
(66) Dev, P.; Agrawal, S.; English, N.J. *J. Chem. Phys.* **2012**, *136*, 224301–224311.
(67) Boese, A.D.; Handy, N.C. *J. Chem. Phys.* **2001**, *114*, 5497–5503.
(68) Delley, B. *J. Chem. Phys.* **2000**, *113*, 7756–7764.
(69) Delley, B. *J. Chem. Phys.* **1990**, *92*, 508–517.